SEPTEMBER 1994

FOM-INSTITUUT
VOOR
PLASMAFYSICA
RIJNHUIZEN

ASSOCIATIE
EURATOM-FOM

FEASIBILITY STUDY FOR A MULTI-CHANNEL PULSED RADAR REFLECTOMETER FOR THE JET DIVERTOR REGION

S.H. HEIJNEN AND M.J. VAN DE POL

RIJNHUIZEN REPORT 94-222

REPORT ON JET ARTICLE 14
CONTRACT NO. JE2/9001

PROJECT LEADER: C.A.J. HUGENHOLTZ

This work was performed as part of the research programme of the association agreement of Euratom and the 'Stichting voor Fundamenteel Onderzoek der Materie' (FOM) with financial support from the 'Nederlandse Organisatie voor Wetenschappelijk Onderzoek' (NWO) and Euratom.

POSTBUS 1207
3430 BE NIEUWEGEIN
NEDERLAND
EDISONBAAN 14
3439 MN NIEUWEGEIN
TEL. 03402 - 31224
TELEFAX 03402 -31204

Contents

1. Introduction

In this report, the feasibility of a pulsed radar system for measuring the electron density profile in the divertor region of JET is studied. In pulsed radar systems, short pulses are launched into the plasma, and the time of flight between emission, reflection from a critical density layer, and detection is measured. Because of the shortness of the pulses, false reflections from e.g. the vacuum window can easily be separated in time from reflections in the plasma. Therefore, one antenna is sufficient for both launching and receiving, making the access demands to a tokamak very limited. An advantage of pulsed radar systems over conventional reflectometer systems is that during the short propagation time of the pulse through the plasma, fluctuations can be regarded to be frozen into the plasma. As each received pulse contains all necessary information to reconstruct the density profile, signal losses will not influence the data interpretation. Also this is an important advantage over conventional reflectometers, especially in the divertor plasma where signal losses will often occur due to the high degree of plasma turbulence.
For the feasibility study, some dedicated experiments are performed with a four-channel system, which was designed for the RTP tokamak (RTP = Rijnhuizen Tokamak Project). To simulate divertor plasmas the measurements are performed in ECRH induced plasmas without current. The parameters of these kinds of plasmas are: $n_e < 3\times10^{19}$ m^{-3}, $T_e < 100$ eV, and a diameter of ≈ 30 cm. This resembles the expected parameters of the divertor plasma very well.
The outline of this report is as follows. In Section 2 the relevant theory of pulse propagation in plasmas is briefly discussed. The RTP pulsed radar system is described in Section 3, while the time-interval counter is presented in more detail in Section 4. In Section 5, special attention is devoted to the resolution of the time-of-flight measurements. In Section 6, measurements done with the pulsed radar system are compared with those of a 19-channel interferometer and a TV Thomson-scattering system. In Section 7 a discussion on the pulse loss rate and the resulting reliability is given. Finally, in Section 8, a design of a multi-channel pulsed radar system for JET is proposed, based on the experience gained with the RTP system.

2. Theory

The plasma refractive index is a complicated quantity which, in general, depends on the magnetic field strength, density and temperature. Here, only propagation of electromagnetic waves perpendicular to the magnetic field, and with the electric field of the wave oriented parallel to the magnetic field (O-mode) is considered. In this case the refractive index, N, has the simple form:

$$N^2 = 1 - \frac{\omega_p^2}{\omega_0^2} = 1 - \frac{n_e}{n_c}, \qquad (2.1)$$

with $\omega_p = 56.38\sqrt{n_e}$ being the plasma frequency, ω_0 the probing frequency and n_c the critical density were ω_0 equals ω_p. Equation (2.1) is only applicable in cold plasmas. For plasmas with electron temperatures exceeding 10 keV, relativistic correction factors should be incorporated [Binds-93]. In RTP and the JET divertor region the electron temperatures are well below 10 keV and therefore, Eq. (2.1) can be safely used. From this equation it can be seen that when the plasma frequency becomes larger than the probing frequency, the refractive index becomes imaginary. This means that the wave is evanescent and is reflected. In reflectometer experiments a microwave beam, typically with a frequency between 10 and 100 GHz, is launched into the plasma and is reflected from a critical density layer. The phase change of this beam originating from the plasma is given by [Ginz-60]:

$$\varphi = \frac{4\pi f}{c} \int_a^{r_c} N \, dx - \frac{\pi}{2}, \qquad (2.2)$$

with a being the edge of the plasma, and r_c being the position where $\omega_0 = \omega_p$. Equation (2.2) can also be used to describe the interaction of short pulses with plasmas. In this case, (2.2) must be evaluated for the whole frequency spectrum of the pulse. In general this is done by Fourier transforming the pulse, calculating the phase change for each individual frequency component and then applying an inverse Fourier transform. In this way both the time delay and the pulse-shape deformation can be calculated for any type of pulse. When Gaussian-shaped pulses are used, some approximations can be made. The pulse can be represented by:

$$E(t) = \frac{A}{\sqrt{2\pi}\,\sigma} \exp\left(-\frac{t^2}{2\sigma^2}\right) \exp(i\omega_0 t), \qquad (2.3)$$

with ω_0 being the probing frequency and σ the width of the pulse. The Fourier image of a Gaussian pulse will also be Gaussian and is given by:

$$F(\omega) = A \exp\left(-\frac{\sigma^2(\omega-\omega_0)^2}{2}\right). \qquad (2.4)$$

If a pulse with a shape given by (2.3) is launched into the plasma, then the received pulse, after reflection from a critical density layer, is given by:

$$E(t) = \int_{-\infty}^{\infty} A \exp\left(-\frac{\sigma^2(\omega-\omega_0)^2}{2}\right) \exp(-i\varphi(\omega)) \exp(i\omega t)\, d\omega, \tag{2.5}$$

with φ given by (2.2). Because the width of the frequency spectrum is usually much smaller than the probing frequency, (2.2) can be Taylor-expanded around the probing frequency ω_0.

$$\varphi(\omega) = \sum_{n=0}^{\infty} \frac{1}{n!} (\omega-\omega_0)^n \varphi^n(\omega_0). \tag{2.6}$$

Here, φ^n denotes the n^{th} derivative of φ with respect to ω. The zeroth-order term gives the phase shift for the carrier frequency. The first-order term gives a phase shift linear in the frequency. This can be associated with the time delay given by:

$$\tau_p(\omega_o) = \frac{\delta\varphi}{\delta\omega_0} = \frac{2}{c} \int_a^{r_c(\omega_o)} \left(1 - \frac{\omega_p^2(x)}{\omega_0^2}\right)^{-0.5} dx. \tag{2.7}$$

The second order term is quadratic in frequency and will therefore directly influence the pulse width. For Gaussian-shaped pulses, and neglecting third and higher order terms in (2.6), it can be shown that the pulse remains Gaussian after reflection. However, the pulse width will increase according to:

$$W_r = W_t \sqrt{1 + \left(\frac{8 \ln 2\, \varphi''(\omega_0)}{W_t^2}\right)^2}, \tag{2.8}$$

with $W_t = \left(\sqrt{8\ln 2}\right)\sigma_t$ being the FWHM of the transmitted pulse, W_r the FWHM of the received pulse, ω_0 the probing frequency and φ'' the second derivative of (2.2) with respect to ω. The pulse remains Gaussian only if the third-order term is small. The third-order term can be associated with asymmetries of the reflected pulse and is given by:

$$\frac{1}{3!}(\omega-\omega_0)^3 \varphi'''(\omega_0) = \frac{1}{3!}(\omega-\omega_0)^3 \frac{6}{c} \int_a^{r_c(\omega_0)} \frac{\omega_p^2/\omega_0^2}{\left(1-\omega_p^2/\omega_0^2\right)^{3/2}} dx. \tag{2.9}$$

In Fig. 2.1, a comparison is made of the different terms in the expansion (2.6) for a parabolic density profile. For the calculations, the probing frequency was held constant and the top density was scanned from 1 till 100 times the critical density. The terms of the expansion are

calculated at a frequency shift from the probing frequency, that corresponds to a level of 1/32 of the amplitude of the electric field of the incoming pulse. Note that this is at the -30 'B level of the power of the pulse, corresponding to a 30 dB on/off ratio o the pulse modulator. The FWHM of the pulse was 700 ps. The third-order term is of the same size as the second-order term for a value of r_c/a equals 0.2. This is at 96% of the top density. In this region, the WKB approximation breaks down, and therefore calculations are not allowed anyhow.

The pulse width for a Gaussian pulse with a FWHM of 700 ps, after reflection from a plasma with a parabolic density profile, is shown in Fig. 2.2. The pulse broadening is calculated using (2.8). It can be concluded that for pulses reflecting from a position in the outer half of the plasma, pulse broadening is small. For positions of the reflecting layer in the centre half of the plasma, the pulse width is rapidly increasing, and corrections for pulse broadening should be made.

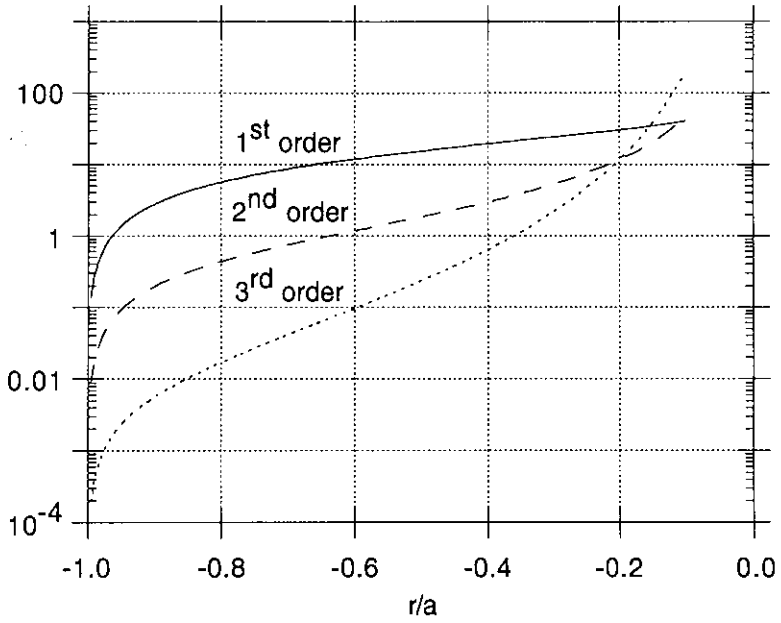

Fig. 2.1: *Values of the different terms in the Taylor expansion of* φ,calculated at $\omega-\omega_0 = 12.3\times10^9$ Hz.

The pulse width for a pulsed radar system operating in the JET divertor region should be a trade-off between a minimum pulse distortion, and having no interference at the antenna between the rising edge of the pulse that is already reflected from the plasma, and the trailing edge of the pulse that still has to leave the antenna. The first means a long pulse, while the last means a pulse length that is shorter than twice the distance between the antenna and the plasma edge. When two antennae are used, the last criterion is not as stringent.

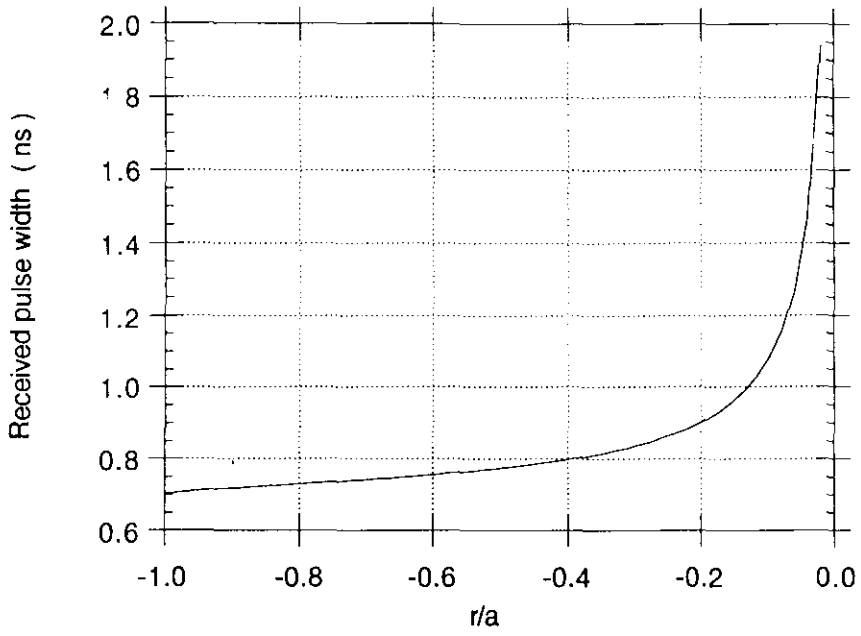

Fig. 2.2: Received pulse width for a transmitted pulse of 700 ps launched into a plasma with a parabolic density profile.

In pulsed radar experiments the time of flight, $\tau(\omega)$, is measured and the "density profile" $r(\omega)$ has to be calculated. This is done by inverting (2.7) using Abel inversion techniques [Budd-61]:

$$r(\omega_0) = \frac{2c}{\pi} \int_0^{\omega_0} \frac{\tau(\omega)}{\sqrt{\omega_0^2 - \omega^2}} d\omega \qquad (2.10)$$

Normally, the time-of-flight profile is measured at a few discrete points only. Between these points the profile has to be interpolated. For the part of the profile below the lowest probing frequency, a physical model describing the time-of-flight profile (e.g. the edge density profile) has to be assumed.

3. RTP pulsed radar system

3.1 General

A four-channel pulsed radar system operating in the Ka-band (26.5 - 40 GHz) was developed for the RTP tokamak. Pulses with a FWHM of 500 ps are launched into the plasma and the time of flight between emission, reflection from a critical density layer, and detection is measured with an accuracy of 70 ps. This corresponds to a spatial resolution of 1 cm when

reflections from a metal mirror in vacuum are measured. The four frequencies of the transmitter are switched sequentially by a single-pole four-throw (SPFT) pin switch. The receiver is heterodyne, combining a large bandwidth with a high dynamic range.
The pulsed radar system at RTP was placed 15 meters away from the tokamak. The transmission line used consists of oversized waveguides and several single-mode bends. In the following sections the different components of the system will be discussed in more detail.

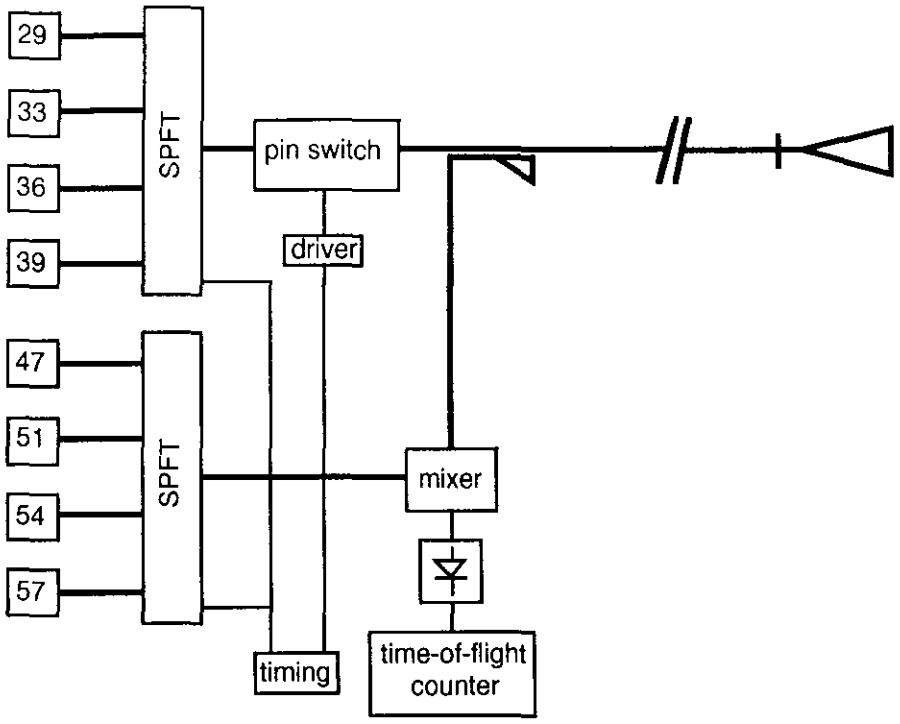

Fig. 3.1.1: The RTP pulsed radar system.

3.2 Transmitter

The four different frequencies are generated by Impatt oscillators with an output power of 200 mW at 29 and 33 GHz and a power of 400 mW at 36 and 39 GHz, respectively. The Impatts are used in a CW mode. The four frequencies are combined into one waveguide using a SPFT pin switch, with an insertion loss of 4.5 dB and an on/off ratio of 25 dB, see Fig 3.2.1. The four frequencies are switched sequentially every 500 ns. Hence, a complete frequency scan is made in 2 μs. The short pulse is formed using a fast pin switch. In the transmission state the diode is biased with +5 V and has an insertion loss <1.5 dB. In the isolation state it is biased with -2 V and has an insertion loss of >35 dB. Therefore the on/off ratio is >33 dB. According to the manufacturer, the rise time of this fast pin switch is 1.5 ns and the fall time 2.5 ns, when use is made of a monopolar driving pulse with an amplitude of 7 V and a DC offset of -2 V. The rise time and width of this driving pulse were 1.5 ns and 10 ns, respectively. To decrease the rise and fall times of the pin switch, a driver from AVTECH was

used. This driver is capable of generating pulses with an amplitude of up to 15 V and a width selectable between 0.2 and 2 ns. Using this driver the rise time can be decreased to 450 ps, but the fall time is still 2.5 ns. To improve the fall time also, a bipolar pulse should be used.

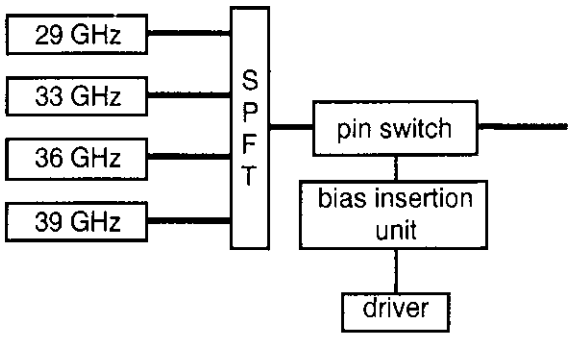

Fig. 3.2.1 Scheme of the transmitter.

This pulse is made using a balanced T, short-circuited on one end. The reflection on this short will give a negative pulse. Together with the original pulse a bipolar pulse is formed. By adjusting the distance between the short and the T, the "width" of the bipolar pulse can be changed. The width is here defined as the time between the maximum and the minimum. The combination of a pin switch with a short-circuit will give large reflections back to the driver, and subsequent reflections from the driver output. Therefore, one driver pulse will yield multiple pulses on the pin switch. To suppress this effect, an attenuator is placed between the driver and the pin switch. Because the switch should be closed between subsequential driving pulses, a DC bias of -2 V is added on top of the driving pulse. The schematic circuit is shown in Fig. 3.2.2. The shape of the bipolar driving pulse could only be measured when it was put directly on a fast sampling scope with a 50 Ω input, see Fig. 3.2.3a. As the impedance of the pin switch changes during switching, the exact shape of the actual driving pulse is unknown. Using this bipolar driving pulse, an RF pulse of 500 ps FWHM could be made, see Fig. 3.2.3b, which is the smallest pulse width that can be achieved with a pin switch. The drawback is an increase in insertion loss.

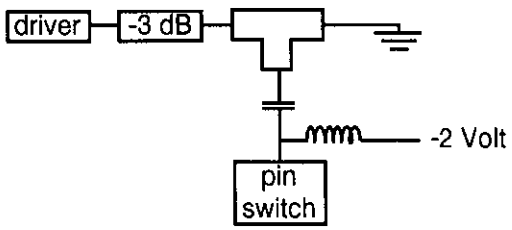

Fig. 3.2.2: Scheme of the pin switch driver.

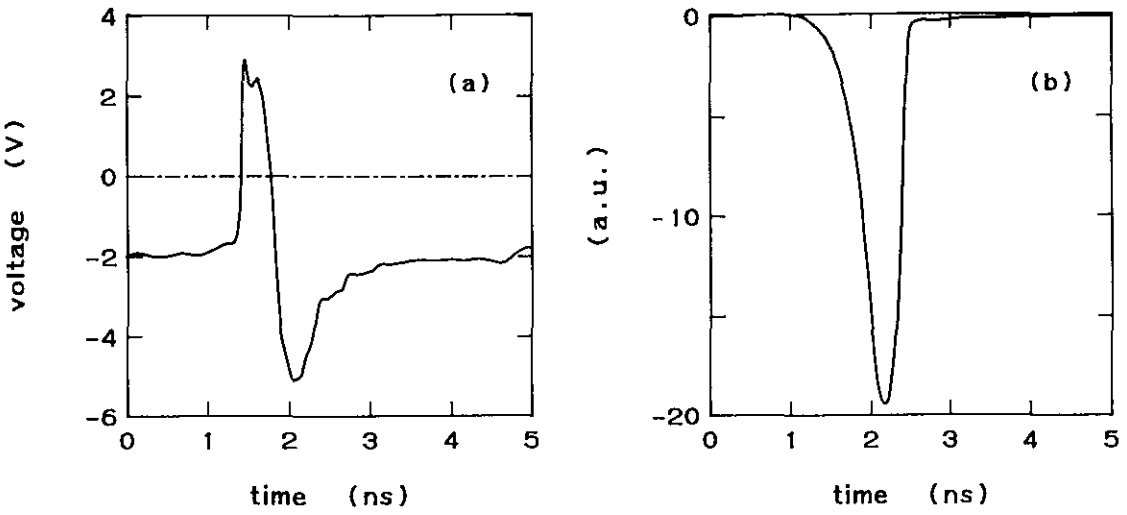

Fig. 3.2.3: (a) Bipolar driving pulse as measured with a fast sampling scope (Tectronix CSA 803), and (b) RF pulse as made by the pin switch.

Therefore, measurements will be performed with pulses with a FWHM of 700 ps. Even then the insertion loss is already 3 dB higher than in CW or long pulse operation.

3.3 Receiver

To receive the pulses reflected from the plasma, heterodyne techniques are applied. This yields a higher dynamic range than when direct detection is used. The local oscillator (LO) which drives the mixer consists of four Impatt oscillators which are switched sequentially by a SPFT pin switch, see Fig. 3.3.1. The LO switches synchronously with the transmitter in such a way that the frequency of the transmitter is always 18 GHz below that of the LO. The conversion loss of the mixer is 7 dB. The IF frequency of 18 GHz is a trade-off between a minimum needed number of oscillations to define a genuine pulse, and a maximum frequency that is technically and economically possible. Before detection, the IF signal from the mixer is filtered and then amplified by 40 dB. After detection the signal is further amplified by another 20 dB. To limit the pulse distortion by the electronics as much as possible, all components have a linear phase response. Therefore, the filter has a Bessel-type characteristic. The 3 dB bandwidth of the filter is 3 GHz.

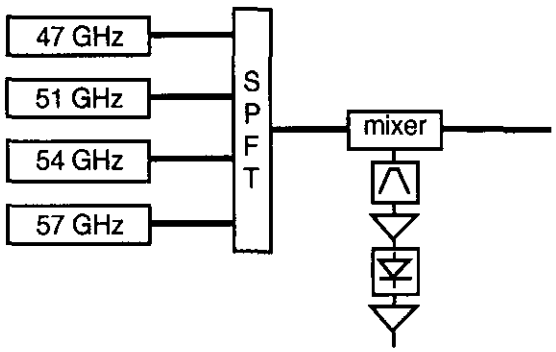

Fig. 3.3.1: Scheme of the receiver.

3.4 Transmission line

To lead the signal from the transmitter to the tokamak and back to the receiver again, oversized waveguides are used. This has two reasons. First, if single-mode waveguide would have been used, the losses would have been unacceptably high: the losses in 30 meters of single-mode waveguide would be 17.4 dB. In oversized waveguide (X-band) the losses are only 3.3 dB, excluding bends. Second, due to dispersion in the waveguides too large a pulse broadening would occur in single-mode waveguides.

The refractive index for the fundamental TE_{10} mode in a rectangular waveguide is given by:

$$N = \sqrt{1 - \left(\frac{\lambda_0}{\lambda_c}\right)^2}\ , \tag{3.4.1}$$

with λ_0 the free space wavelength, and $\lambda_c = 2a$ the cutoff wavelength of the guide. Here, a is the dimension of the waveguide perpendicular to the electric field. Using formulas (3.4.1) and (2.8), it can be shown that the pulse broadening in the waveguide is given by:

$$W_r = W_t \sqrt{1 + \left(\frac{2L \ln 2}{\sqrt{\pi}\, c W_t^2} \frac{f_c^2}{(f_0^2 - f_c^2)^{1.5}}\right)^2}\ , \tag{3.4.2}$$

with L the length of the guide, f_0 the probing frequency and $f_c = c/\lambda_c$ the cutoff frequency of the waveguide. Using (3.4.2), it follows that in fundamental waveguide (Ka-band, 7.112×3.556 mm^2) a pulse of 33 GHz and 700 ps FWHM will broaden to 3.12 ns, while the same pulse in oversized waveguide (X-band, 22.86×10.16 mm^2) will broaden to 714 ps.

The waveguide system consists in total of 30 meters of oversized waveguides (X-band) and several single-mode bends. Furthermore, use is made of two low-pass filters to protect the system from high-power ECRH radiation, two vacuum breaks in fundamental waveguide, 3 meter of fundamental waveguide and two standard gain horns both with a gain of 20 dB. Four of the single-mode bends are complicated bends for they bend ± 20° in the E-plane and ± 30° in the H-plane. The total theoretical losses in the waveguide system are summarized in Table 3.4.1. The total measured round trip loss was 40 dB when reflecting from the back wall of the tokamak. The 5 dB difference between the theoretical and the experimental losses can be explained by in-vessel components giving lower reflections than the back wall.

Instead of using single-mode bends, also oversized mitre bends could have been used. The mode-conversion losses in dB for perfect 90° mitre bends are given by $1.96 \times (\lambda/b)^{0.5}$ for the E-plane, and $2.05 \times (\lambda/a)^{1.5}$ for the H-plane bend. Experiments have shown that these formulas provide accurate results when the values (λ/b) and (λ/a) are less than 0.4 [Okre-68].

	Theoretical (in dB)
transmitting waveguide	-4.0
2 complex bends	-1.0
vacuum break	-1.0
loss between transmitting and receiving antenna	-22.9
vacuum break	-1.0
receiving waveguide	-4.0
2 complex bends	-1.0
total	-34.9

Table 3.4.1: Theoretical losses in the waveguide system.

For longer wavelengths measured values of mode-conversion losses are smaller than the calculated values. For X-band at 33 GHz the theoretical losses per mitre bend are 1.85 dB for the E-plane and 0.51 dB for the H-plane. The measured losses in these bends were 0.7 dB for the E-plane and 0.3 dB for the H-plane. At JET, S-band bends are being used. In that case losses are 1.01 dB in the E-plane and 0.1 dB in the H-plane. Pulse-shape deformation in both X- and S-band bends were hardly detectable and therefore negligible.

4. Time-of-flight measurements

4.1 General

For studying the feasibility of a pulsed radar reflectometer for JET and future fusion devices, a high-resolution time-of-flight measurement set-up with a high repetition rate is needed. A temporal resolution of 70 ps is required, corresponding to approximately 1 cm spatial resolution when reflections from a metal mirror in vacuum are measured. This resolution, in combination with a repetition rate > 2×10^6 measurements per second, cannot be obtained by means of commercially available time-interval counters. At FOM Rijnhuizen a new time-interval counter is being developed, based on the principle of counting gated clock pulses simultaneously by eight parallel counters. This chapter contains the design considerations and description of this system and the first results.

4.2 Methods to measure time intervals

Many systems for time-interval measurements are based on the principle of counting gated

clock pulses during the time between a stop and a start event. The resolution of such a system will be equal to one clock period, due to the ± 1 count ambiguity. If the fastest presently available digital electronics is used (NEL GaAs), a resolution of approximately 200 ps will be the limit.
Two techniques are often used to improve the resolution:

- interpolation techniques;
- averaging of several successive measurements.

Interpolation techniques, like linear interpolation (used in the HP5334B) and Vernier interpolation (used in the HP5370B) exploit the extra information about the threshold crossings of the input signal relative to the clock signal. By averaging several successive measurements, the result is improved by a factor equal to the square root of the number of measurements, provided only that the repetition rate of the start pulses is non-synchronous with the clock pulse rate.
Both techniques have the disadvantage of a decrease of measurement rate. Therefore, we use a different approach, which can be understood as a parallel averaging method. A clock is supplied with a fixed relative phase shift to eight parallel counters. The measured time interval is equal to the average of the outputs of the counters, with a maximum resolution equal to one clock period divided by the number of counters. This system will be described in more detail in paragraph 4.4.

4.3 Time-pickoff techniques

In all time-interval measurement systems, the occurrence of a start and a stop event must be precisely related in time to the start or the end of the measurement by means of a time-pickoff element [EG&G-82]. Three important sources of error can introduce uncertainties in a time-pickoff measurement: walk, drift and jitter.
Walk is the time movement of the output pulse from the pickoff element, relative to its input pulse, due to variations in the shape and amplitude of the input pulse. Drift is the long-term timing error introduced by component ageing and by temperature variations in the time-pickoff circuitry. Jitter is the timing uncertainty of the pickoff signal that is caused by noise in the system and by statistical fluctuations of the input signals.
The accuracy of pulsed radar measurements is influenced negatively by walk and jitter. The amplitude fluctuations of the pulse which is reflected at the critical density layer in the plasma can be very large, especially in turbulent plasmas. Because of dispersion in the plasma, the pulse will also broaden. However, pulse broadening is not expected to play a significant role in small tokamaks with high density gradients, like RTP, or in the JET divertor plasma. The effect of noise-induced errors on the measurement accuracy of a pulsed radar system will be large compared with a CW reflectometer system, because a pulsed radar system needs a larger detection bandwidth in order to detect short pulses. This is analysed in Chapter 5. In most

detection bandwidth in order to detect short pulses. This is analysed in Chapter 5. In most cases, drift will not hamper the measurements because the system can be calibrated easily before every tokamak discharge, using the reflection on the back wall of the tokamak vacuum vessel as a reference. However, drift of the counter clock frequency must be avoided, because of the frequency-dependent tuning techniques, which are used in the counter system. Checking and tuning of the voltage-controlled clock oscillator will be necessary on regular intervals.
Three techniques for time-pickoff elements are commonly used:

- leading-edge discriminators;
- true constant-fraction discriminators (TCF);
- amplitude-and-rise-time compensated discriminators (ARC).

Leading-edge discriminators trigger at a constant voltage level. TCF and ARC discriminators trigger at a constant fraction of the pulse amplitude. TCF timing is most effective when used with input signals having a wide range of amplitudes but a narrow range of rise times and pulse widths. The timing error due to noise-induced jitter for TCF timing is worse than for leading-edge timing, but better than for ARC. Because of the insensitivity for amplitude fluctuations, TCF discriminators are the best choice for pulsed radar at RTP. At larger tokamaks, where pulse broadening will be significant, ARC is a better choice, because this technique is most effective when used with input signals having a wide range of amplitudes and rise times.
The measurements, presented in this report, are performed using a Model 2126 constant-fraction discriminator (Canberra-Packard). This discriminator has an input range from -5 mV to -5 V. Over this dynamic range the walk will be less than 100 ps.

4.4 RTP time-interval counter

The time-interval counter, developed at Rijnhuizen, employs eight parallel gated six-bits ripple counters, see Fig. 4.4.1. The gates are opened simultaneously during the time-interval between the start and the stop pulse. The reflection from the vacuum window can be used as a start pulse in case of a single antenna set-up. The clock is phase shifted by n×45°, with n = 0,1,..,7. The measured flight time of the pulses will be equal to the average of the output of the eight counters, with a resolution improved by a factor of eight. The amount of data is reduced by adding the output of the counters. After the addition, data is stored into a VME memory module via an interface, synchronizing the control clock of the measurement system with the central RTP or JET data-timing clock.
The clock frequency of the counters is 1.8 GHz, the maximum frequency at which the fastest ECL family (SELIC, manufactured by NTT Electronics Technology Corporation, Japan) can operate. SELIC was chosen instead of the faster GaAs electronics because SELIC is cheaper and easier to implement. The resolution of the system is expected to be $\pm$ 69 ps. The maximum time-interval which can be measured is 35.5 ns.

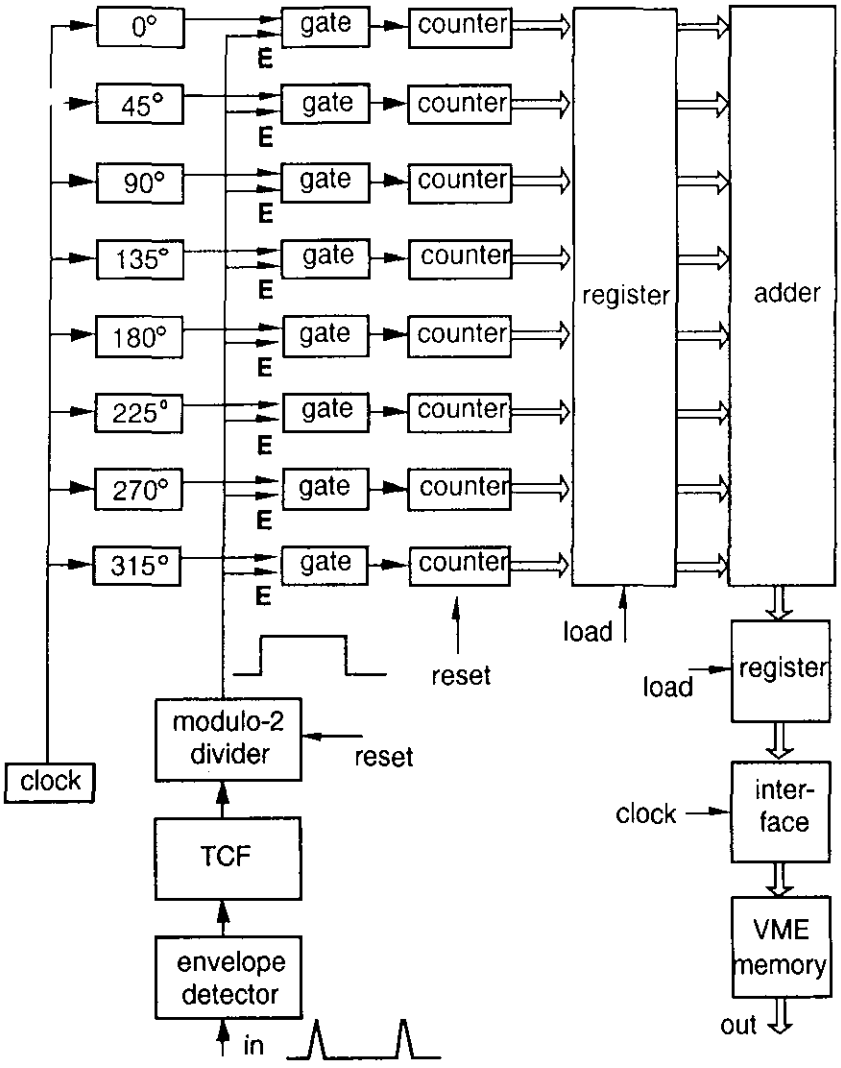

Fig. 4.4.1. : Time-interval measurement with parallel averaging.

The layout of the printed circuit boards of the counter system was designed using the general purpose programme PCAD. All on-board high-speed connections were made by 50 Ohm UT-34 semi-rigid cables, terminated into 50 Ohm resistors.

The measure sequence is controlled by a 32 Mc crystal oscillator and a Johnson counter with 16 outputs, yielding a total time of 500 ns to perform one measurement. The timing diagram is depicted in Fig. 4.4.2.

Every sequence is started with the setting of both multi-throw pin switches in the transmitter and receiver of the pulsed radar system. After four sequences these pin switches are in their initial position again. After the setting of the multi-throw pin switches, the modulo-2 divider and the counters are reset, followed by the triggering of the fast pin switch. After measuring the time interval between the start pulse from the vacuum window and the stop pulse from the plasma, taking into account a maximum round-trip delay of 125 ns including the measurement duration, the output of the counters is loaded into a register. The output of the adder is also

stored into a register. The time difference between the loading of both registers is needed to overcome the propagation delay of the adder. At the end of the sequence, data is clocked into a VME memory. The measurement rate, resulting from this sequence, can be improved by building a faster adder such that every new sequence can start already after eight control clock pulses instead of 16, because the temporary storage into a register before the adder would become superfluous.

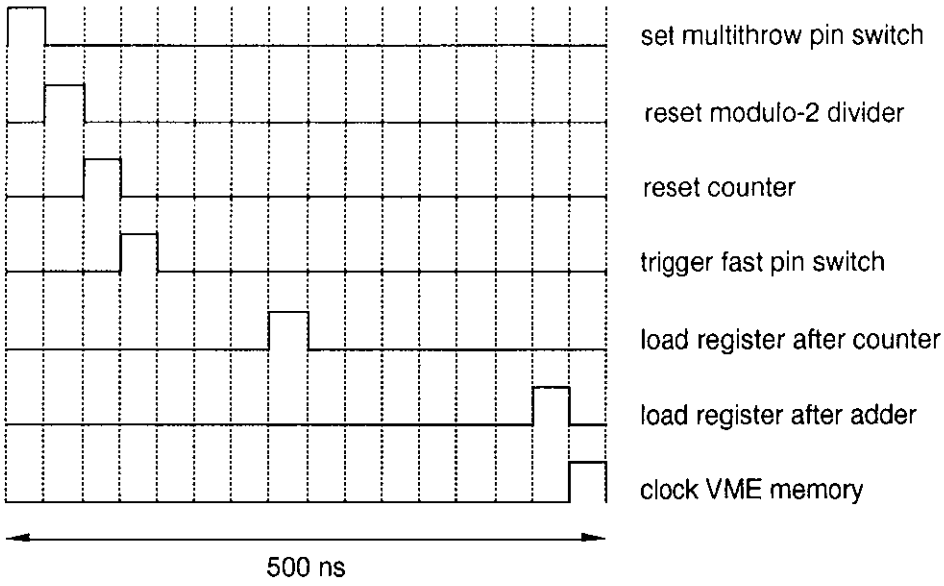

Fig. 4.4.2: Time diagram of the time-interval counter.

4.5 Performance tests

To check the performance of the counter system, the output of the adder was supplied to a digital-to-analog converter (DAC). The output of this converter was displayed on a Tektronix 475 oscilloscope.

First, the system was tested with a single ripple counter, by varying the gate time in which the counter accepts clock pulses. The scope clearly showed the quantization of the converter output, corresponding to the number of counts of the ripple counter. The ± 1 count ambiguity was measured over the complete time-interval input range from 0 to 35.5 ns.

Next, two counters were connected. The clock which was applied to the second counter had a phase shift of approximately 180°. The output range of the DAC was doubled, without an increase of count ambiguity. This result confirms the principle on which the counter design is based.

Next, four ripple counters were implemented. The clock was phase-shifted approximately n×90°, with n = 0,1,..,3. The output range of the DAC increased by a factor of four, as expected, but the scope showed four quantization levels instead of three, at discrete input time intervals when the time interval is equal to an integer times one quarter of the clock period. This

unintended increase of count ambiguity is probably caused by an insufficient accuracy of the clock phase-shift. In the current design, the phase of the clock is shifted by tuning the length of a coax cable. A more accurate method has been found and is in the process of being implemented.
Because of the problem mentioned above, a complete counter system with eight ripple counters could not be tested yet.

5 Resolution

In this chapter, the resolution of pulsed radar systems is taken into consideration. The hardware resolution is set by the counter system. In our case this is ± 70 ps. Another limit is set by the signal-to-noise ratio.
The most difficult components for calculating the signal-to-noise ratio are in the receiver. Namely the mixer followed by a matched bandpass filter and a detector. In our case this is a squared law detector. Suppose that the mixer output gives Gaussian-shaped pulses and a spectrum of white noise. The pulse can be represented by:

$$s(t) = \frac{\alpha}{\sigma\sqrt{2\pi}} \exp\left(-\frac{t^2}{2\sigma^2}\right) \cos(\omega_0 t), \tag{5.1}$$

with $\alpha/\sigma\sqrt{2\pi}$ being the pulse amplitude and σ defining the pulse width. The noise has a spectral power density given by:

$$P_n(\omega) = \frac{\eta}{2}, \tag{5.2}$$

with η in W/Hz. After some mathematics, the signal-to-noise ratio is given by:

$$SNR = \frac{\alpha^4\sqrt{2\pi}}{32\pi^2\sigma\eta\left(\eta + 2\alpha\sqrt{\frac{2\eta}{7}} + \frac{\alpha^2}{2\sqrt{3}}\right)}. \tag{5.3}$$

In the limit of high signal-to-noise ratios this can be simplified to:

$$SNR = \frac{\alpha^2\sqrt{6\pi}}{16\pi^2\sigma\eta} = \left(\sqrt{\frac{3}{2\pi}}\frac{\sigma}{4}\right)\left(\frac{\alpha^2}{4\pi\sigma^2}\right)\left(\frac{2}{\eta}\right). \tag{5.4}$$

In (5.4) the first term between brackets denotes an integration bandwidth, the second term is the square of the pulse amplitude and represents the pulse power, and the third term between brackets denotes one over the noise's spectral power density.

Noise on the reflected pulse gives an error in the timing. The jitter coming from this depends on the SNR, the rise time of the pulse, and the triggering level at which a time point is marked. For Gaussian-shaped pulses it can be shown that at 60% of the maximum, the slope of the pulse is highest and the effect of the signal-to-noise ratio is minimum. This level is taken as time mark for the stop pulse. The timing accuracy is given by:

$$\delta t = \frac{\sqrt{2}\, e^{0.5}\, \sigma}{\sqrt{SNR}} . \qquad (5.5)$$

So, to get a spatial resolution of 1 cm in vacuum, this means a timing resolution of 70 ps, with a pulse of FWHM = 500 ps; the SNR should be: 50 or 17 dB.
In the RTP system, transmitters with a power of 23 dBm at 29 and 33 GHz and a power of 26 dBm at 36 and 39 GHz are used. Both the SPFT and the fast pin switch have a loss of 4.5 dB. The mixer in the receiver has a conversion loss of 7 dB. Together with the (measured) losses in the waveguide system a round trip loss of 56 dB has to be overcome. Therefore the signal power at the output of the mixer is: -33 dBm.
Several sources of noise are important for the system. One is the noise from the plasma. In a thermal plasma with a temperature of 1 keV and no suprathermal electrons present, this is estimated to be about 1.6×10^{-19} W/Hz. This has to undergo the loss in half of the waveguide system and the conversion loss of the mixer. Thus, the noise power coming from the plasma after the mixer is: 1.13×10^{-20} W/Hz. Another noise source is the mixer. The noise figure is about the same as the conversion loss. Therefore, the noise produced by the mixer is: 2.0×10^{-20} W/Hz. So, the total noise power coming from these sources is: 3.1×10^{-20} W/Hz. Using formulas (5.4) and (5.5), the maximum SNR is 1173 and the maximum time resolution would be 20 ps. This has only a small influence on the resolution set by the hardware.
Two other sources of noise are the on/off ratio of the fast pin switch, and the isolation of the SPFT pin switch. The on/off ratio of the fast pin switch is not expected to give any problems. Because of the limitation in the on/off ratio, a constant signal is sent into the plasma where it will reflect and be detected again. This power will be added to the pulse. The frequency spectrum of this spurious reflected power has no significant contributions above 1 MHz. Because the receiver has bandpass amplifiers between 1 MHz and 1.5 GHz, it will not be seen. The limited isolation of the SPFT pin switch is something completely different. Because of the limitation in the isolation, pulses will be launched at different frequencies at the same time. These pulses can interfere with each other, but because a bandpass filter is used after the mixer, the different pulses will be filtered out and only the one pulse which should be measured is seen. Hence, these two additional sources of noise will not decrease the signal-to-noise ratio.

6 Measurements

In this paragraph, results from the four-channel pulsed radar system at RTP are presented. The measurements were performed in December 1993. Results will be presented for two types of discharges, namely: a standard discharge with a plasma current of 115 kA and an ECRH discharge without plasma current. The first type of discharge is to show the reliability of the pulsed radar system. The last type of discharge is chosen to resemble a JET divertor plasma, and will therefore give an indication of the feasibility of pulsed radar for application in the JET divertor region.
For the Ohmic tokamak discharge a comparison between pulsed radar results and those from a 19-channel interferometer and a TV Thomson system is made. For the ECRH discharges no Thomson data is available and only a comparison with interferometer data is made. All discharges were done in hydrogen unless specifically stated otherwise.
The fast digital counter system presented in Section 4 was not yet operational when the measurements were performed. Instead an analog Time to Amplitude Converter (TAC) was used. The resolution of this TAC is ± 70 ps, which is the same as the design criteria for the digital time-interval counter, only the repetition rate is a factor of four slower. The digital counter system depends on a start and a stop pulse coming from one detector. The TAC has two separate inputs for the start and the stop pulse. The start pulse is coming from a control clock, while the stop pulse is the detected pulse. The CFD used until now needs a pulse of 3 ns. Therefore, the measurements presented here are performed using two separate antennae for transmitting and receiving. Although this is not the design which was shown in Chapter 3, it will still show the possibilities of pulsed radar.

6.1 Density profiles in standard tokamak discharges

The tokamak discharge is characterized in Fig. 6.1.1 where the plasma current, the loop voltage, the horizontal position as deduced from the magnetics, and the central line integrated density are shown. The raw data for the 33 GHz channel of this discharge is shown in Fig. 6.1.2. During the discharge some pulses are not detected by the receiver. This shows up as the data points at zero voltage. This loss of pulses will not hamper the data interpretation. It is clearly visible that the spread in the data points before the discharge ($t < 0.0$ s) is much smaller than during the discharge. In Fig. 6.1.3 the time-of-flight distribution before and during the discharge is plotted and a Gauss curve is fitted to the data points. From this plot it can be concluded that the spread in the data before the discharge is about 20 ps, while during the discharge it becomes 410 ps. This is the same for all four channels. From the raw data, all the points that represent a reflecting position outside the vacuum vessel are removed. On the remaining data points a moving average over ten points is applied. The result is shown in

remaining data points a moving average over ten points is applied. The result is shown in Fig. 6.1.4, for all four channels together.

Each trace of the flight time versus time into the discharge shows three characteristics. Before the discharge, reflection from the back wall is measured. During build-up of the density after break-down, the plasma has not yet reached the critical density, and still reflections from the back wall are seen. During this building up of the density the optical path length increases with the density and it seems like the back wall is moving backwards. When the plasma reaches the critical density, a sudden jump in the flight time occurs. This happens earlier for the lowest frequency than for the highest frequency. This is best visible for the 36 and 39 GHz channels. When the central density exceeds the critical density, reflections from the plasma are measured.

To calculate the position of the reflecting layers, an Abel inversion is performed (Eq. (2.5)). A linear interpolation is applied between the data points. For the part below the lowest frequency, the following assumption is made. The density at the limiter radius is put to zero, and the profile between the limiter and the lowest frequency is again linearly interpolated. The result of the inversion is shown in Fig. 6.1.5 for a time window of 120 to 160 ms. In this plot also the position of the critical density layers as calculated from the interferometer data is shown. It can immediately be concluded that on average the comparison between the two diagnostics is good but that the results from pulsed radar show much more structure. The correlation between the four channels is coming mainly from the linear interpolation between the edge of the profile and the 29 GHz channel combined with the Abel-inversion procedure. In Fig 6.1.6, the profiles from the interferometer, the TV Thomson system, and the pulsed radar system are compared for one time slice. The pulsed radar data are averaged over 10 ms. Again the various diagnostics are in good agreement. Therefore, it can be concluded that the density profiles as calculated from the pulsed radar system can be trusted with an error-bar of about 1 cm. Fluctuations on a scale smaller than 1 cm should be looked at with some scepsis because they will be a mixture of artefacts from the data analysis method and some genuine density fluctuations.

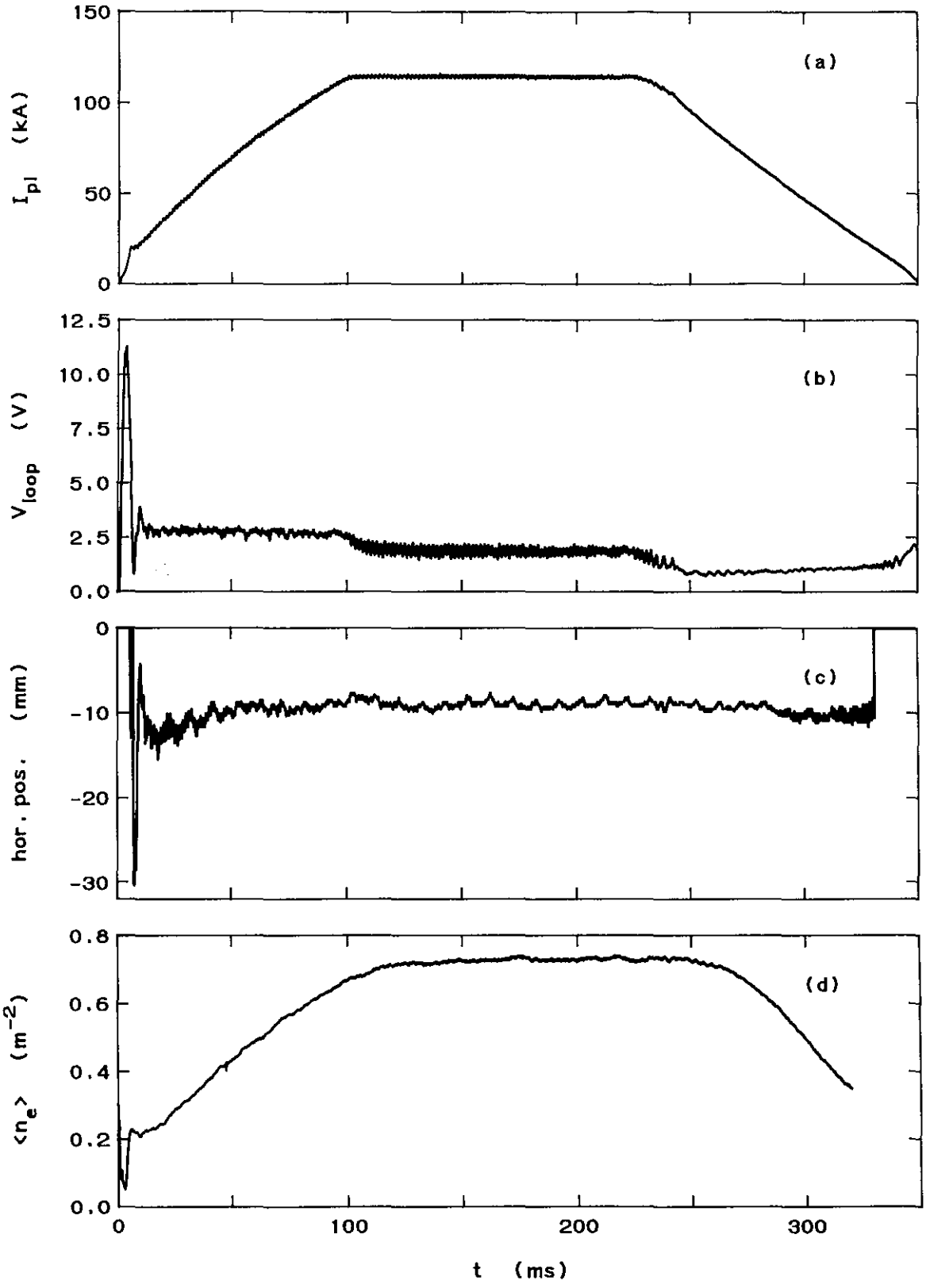

Fig. 6.1.1: Characteristics of the discharge: plasma current (a), loop voltage (b), horizontal plasma position as deduced from magnetics (c), central line integrated density (d).

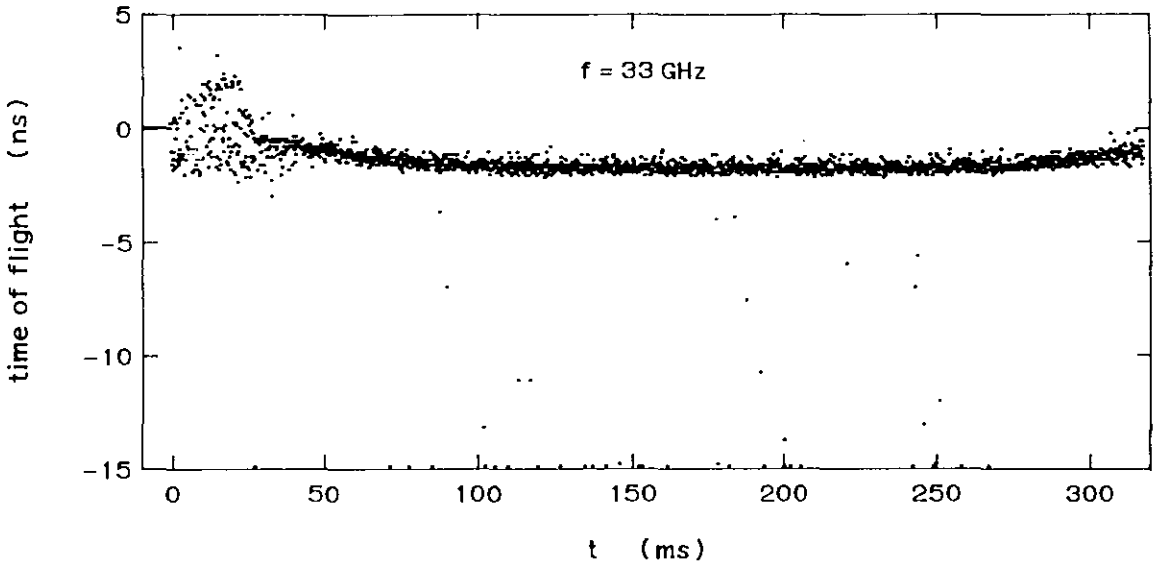

Fig. 6.1.2: Raw data for the 33 GHz channel.

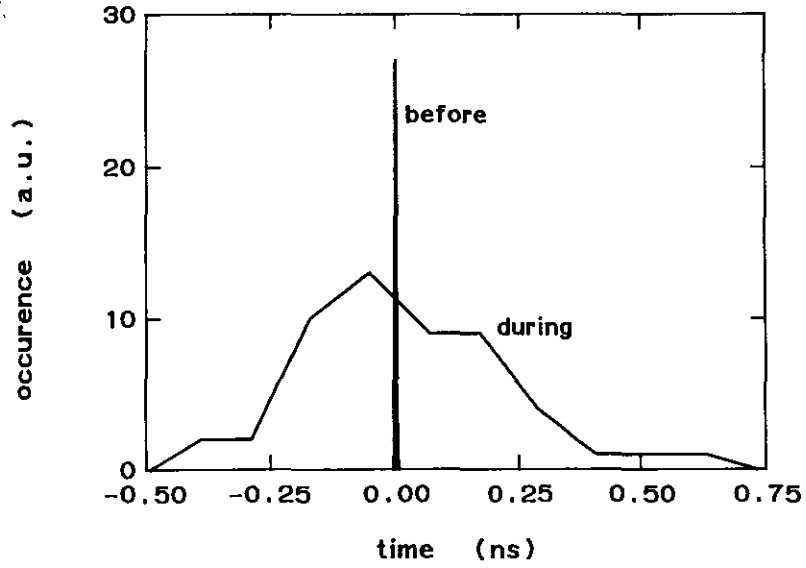

Fig. 6.1.3: Time-of-flight distribution before and during the discharge.

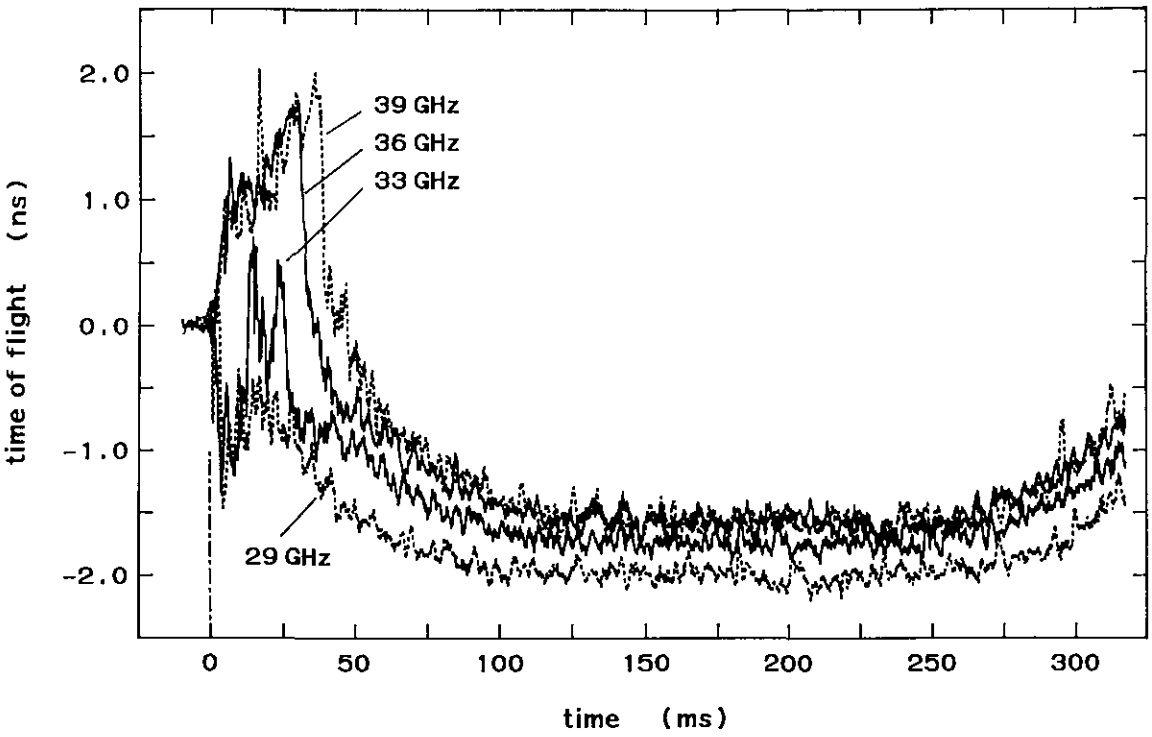

Fig. 6.1.4: Time traces of the four channels from the pulsed radar system after averaging over 10 data points.

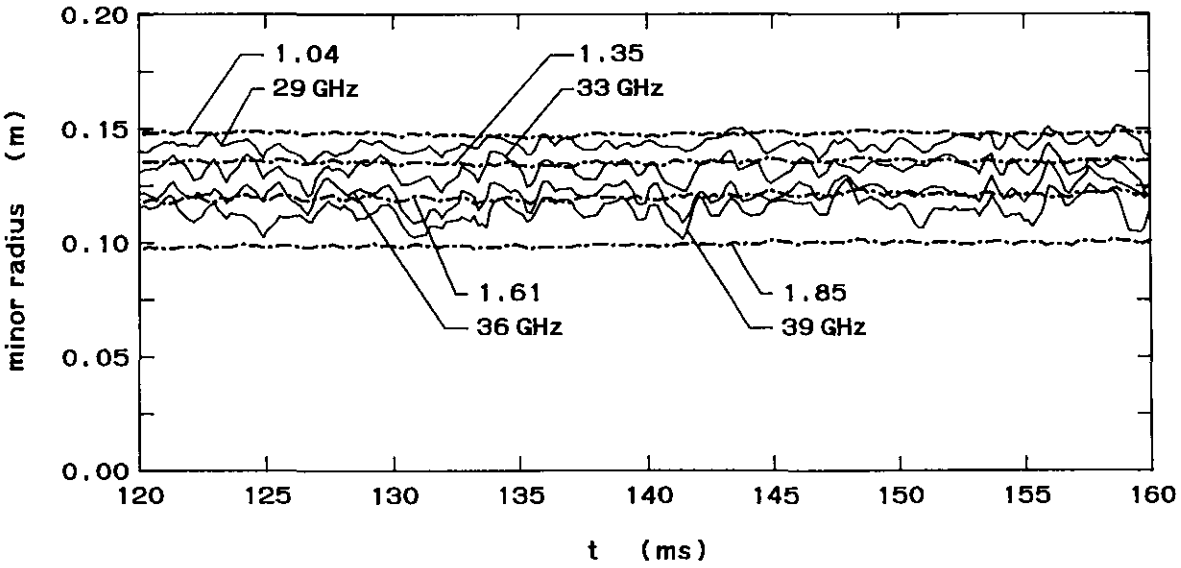

Fig. 6.1.5: Comparison of the density traces as calculated from the pulsed radar system with the density as deduced from the interferometer. The dashed lines represent the interferometer data, while the full lines represent the pulsed radar data.

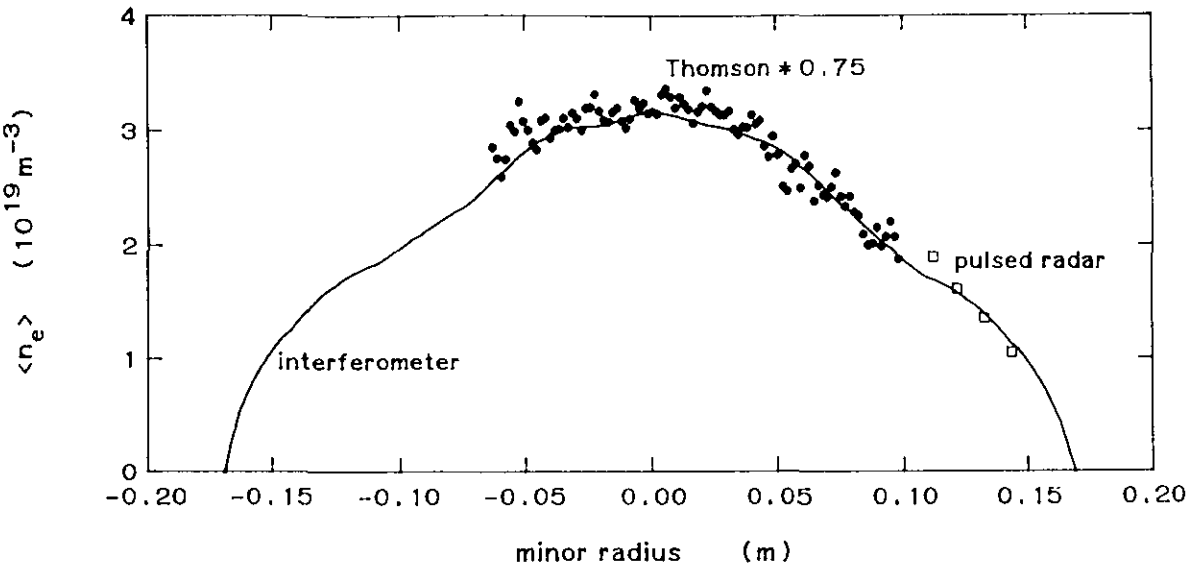

Fig. 6.1.6: The density profiles from the TV Thomson system, the interferometer and the pulsed radar system at t = 140 ms.

6.2 Density profiles in ECRH discharges

In the JET divertor region, plasmas with a temperature of about 100 eV and a density of up to 5×10^{19} m^{-3} are expected. The JET divertor plasma will have a diameter of approximately 30 cm. This type of plasma is well represented by a currentless ECRH plasma in RTP. To have a resonant condition for EC absorption, a toroidal magnetic field was applied. No horizontal or vertical fields were used. Two discharges will be shown here. First, results from a helium discharge, and second, results from a hydrogen discharge are shown.

From earlier experiments at RTP it was already concluded that ECRH plasmas in helium are of relatively constant density. This also shows up from the results with pulsed radar. A constant time-of-flight during the whole discharge is measured, see Fig. 6.2.1. The density profile as calculated from the time of flight is shown in Fig. 6.2.2. Because in these asymmetric plasmas it is not allowed to do an Abel inversion on the interferometer data, the density profile as calculated from the pulsed radar data is compared with the phase profile as measured with the interferometer. From this comparison it can be concluded that both diagnostics measure a relatively constant density profile.

A completely different situation occurs when hydrogen is used. Because hydrogen is not contained as well as helium is, the density in the discharge starts to decay early. The scattering in the data points however, is about the same for both discharges, see Fig. 6.2.3. This indicates that the small-scale turbulences in both discharges are of the same order of magnitude. In the hydrogen discharges the pulsed radar system could show its strength. From the measurements it was possible to follow the density profile in time, although the central density was only during a short period above critical.

The density profiles as calculated from the pulsed radar measurements are shown in Fig. 6.2.4. Here it is assumed that after 10 ms, the central density of the plasma is below critical, and no reflection from the plasma takes place.

From Fig.6.2.3 it can be seen that after 10 ms the 33 GHz channel still shows a lot of measurements with a flight time as if the plasma density was still above critical. This phenomenon is not yet understood. One possible explanation was suggested by Dr C. Laviron. He supposed that a background plasma with a flat density profile with maximum density below 1×10^{19} m^{-3} still existed. This would mean that all the channels would look through the plasma and reflect from the back wall of the vacuum vessel. On top of this background plasma he supposed a small and asymmetric increase in the density up to a value between 1.35 and 1.8×10^{19} m^{-3}. This part of the plasma is assumed to rotate around the center of the vessel. Because of its rotation, this plasma will be seen by the 33 GHz channel only in the few occasions when it is placed exactly in front of the antennae. Because of the flatness of the density profile of the background plasma, the 29 GHz signal will be lost due to the refraction of the plasma when the increase in the plasma is in front of the antennae. This model could explain the double valuedness of the 33 GHz channel and the increase of signal loss for the 29 GHz channel.

Another explanation could be a flat density profile, with a maximum of 1×10^{19} m^{-3}, in combination with a non-constant output power of the gyrotron. This would mean that the deposited power and therefore also the density profile, will be modulated. Because, the deposition profile of the gyrotron power is very localized, the density modulation will also be localized. The measurements can be explained if the increase in the density exceeds 0.4×10^{19} m^{-3}. Again, the loss of signal for the 29 GHz channel would originate from refraction.

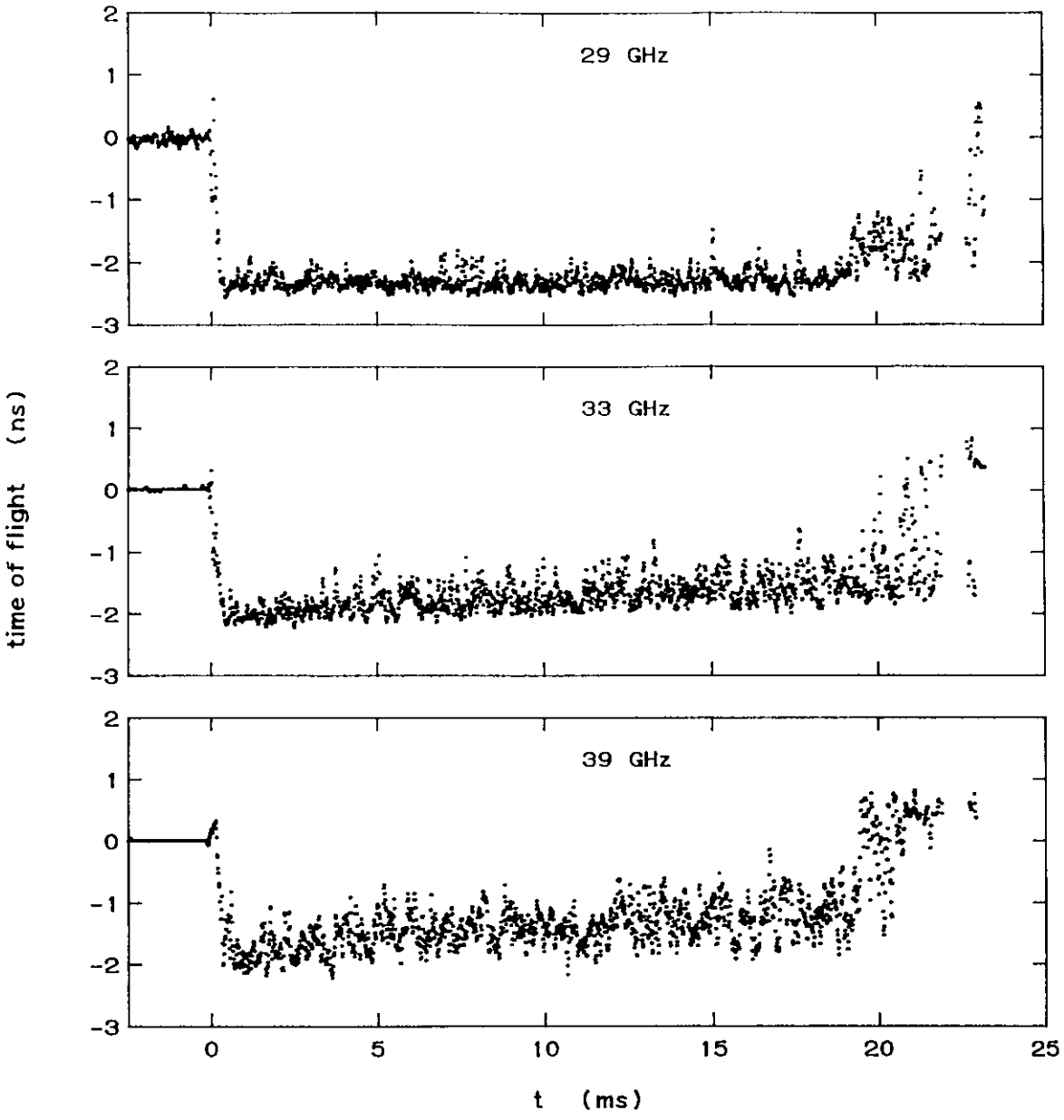

Fig. 6.2.1: Measurements with pulsed radar in a helium ECRH discharge.

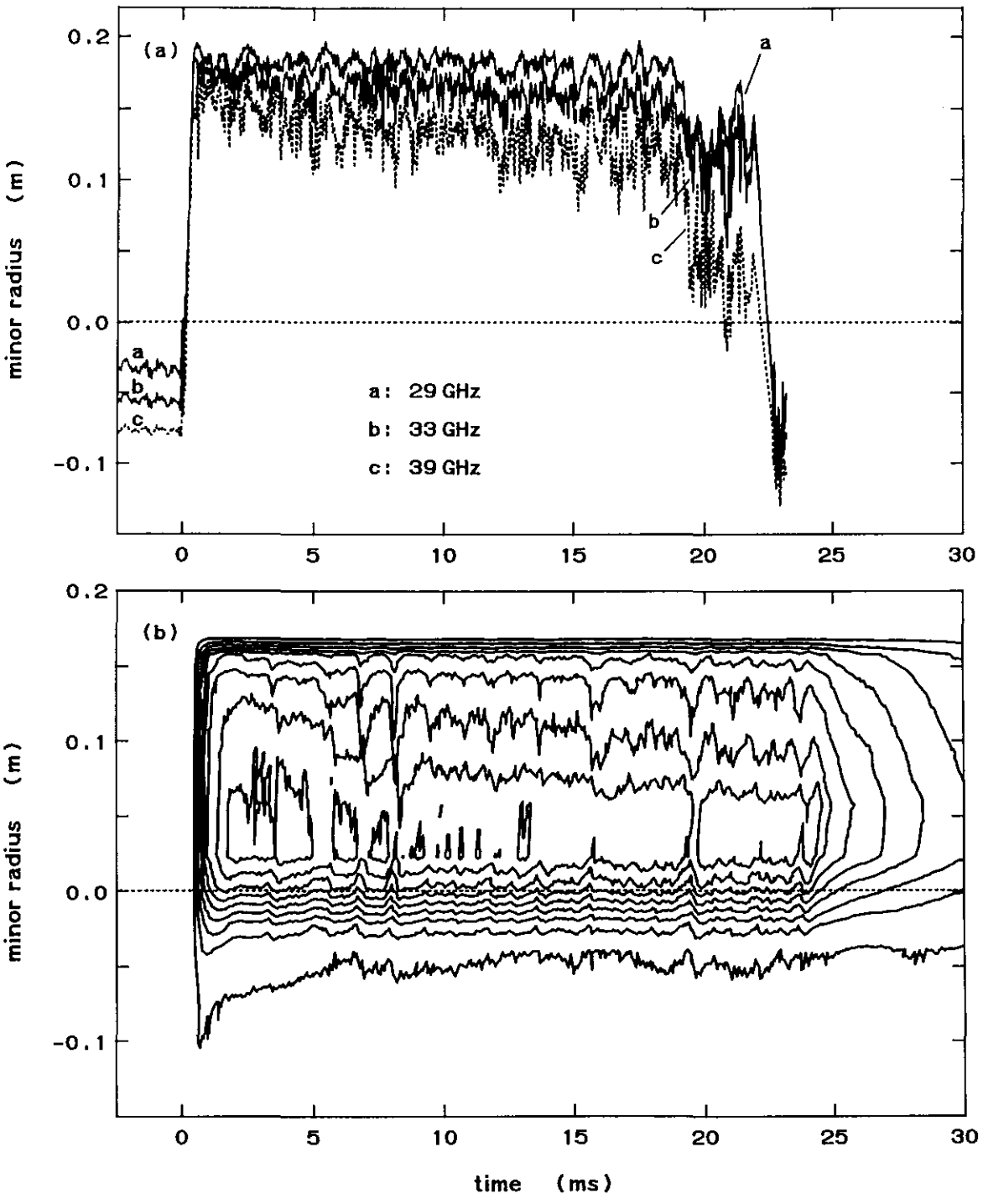

Fig. 6.2.2: *In (a) the density profile as calculated from the measurements in Fig. 6.2.1, and in (b) the phase profile as measured with the interferometer are shown.*

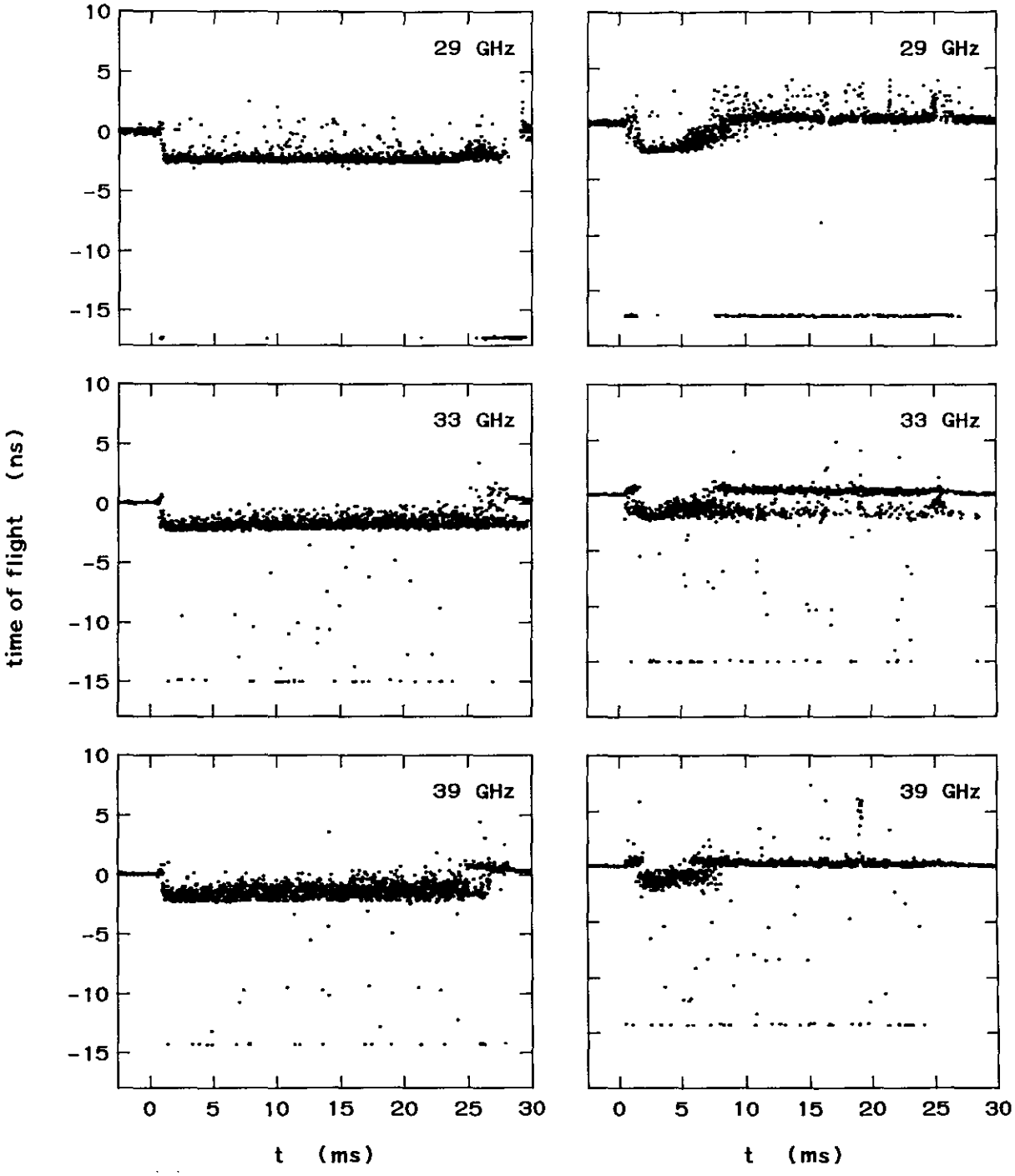

Fig. 6.2.3: Raw data as measured with the pulsed radar system in a helium discharge (left) and in a hydrogen discharge (right).

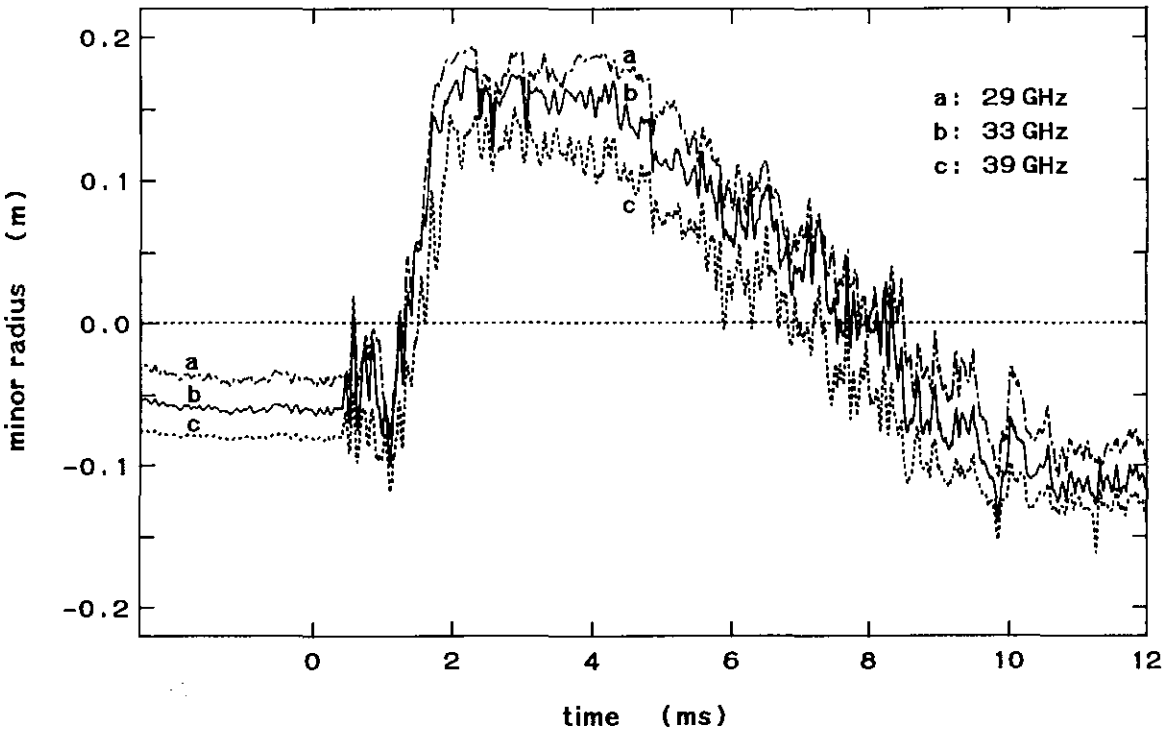

Fig. 6.2.4: The density profile in a hydrogen ECRH discharge.

7 Reliability discussion

Measurements done with a pulsed radar diagnostic are influenced by several factors that will have their effect on the reliability and trustability of the results. On the one hand, too low a reflected signal from the plasma will not trigger the CFD; on the other hand, too high a signal will cause the amplifiers to clip. Because of this, the received pulse will broaden and this will trigger the CFD too early. Also pulse shape deformations can influence the accuracy in the time-interval measurements. This effect will not play an important role on small tokamaks when the outer half of the plasma is probed. When the centre half is being probed, the measurements must be corrected for the pulse broadening. See Chapter 2.

The maximum reflected signal that can be expected from the plasma will occur when a perfect reflecting layer is placed at the edge of the plasma. In this case the round trip losses will be: -30 dB. Then, the signal coming out of the mixer will be -23 dBm. This is too much for the IF pre-amplifier, and it will clip, resulting in a deformation of the received pulse. The plasma will not behave as a perfect mirror, therefore the round trip loss will be higher than -30 dB. Nevertheless, one should always be aware of this effect because it can lead to misinterpretation of the data. It can be avoided if besides the time of flight, also the amplitude of the reflected pulse is detected.

The largest problem in interpreting the data from reflectometers, is the amount of signal loss. In pulsed radar systems this will not be a problem because each received pulse will contain all

necessary information. This remains true as long as there are enough received pulses. As can be expected, the amount of loss depends on the central density. In Fig. 6.1.2 it can be seen that from 50 ms onwards the data can be trusted because the spread in the data points becomes small. At this moment, the central density is above 2.7×10^{19} m^{-3}. In the remaining part of the discharge, when the density becomes even higher, the percentage of signal loss is constant and about 2.5%. There seems to be no dependence on the central density once it is above 2.7×10^{19} m^{-3}. In the case of ECRH discharges, the percentage of signal loss is of the same order of magnitude. The percentage of signal loss can be reduced by increasing the dynamic range of the receiver. This can be done by applying logarithmic amplifiers. Unfortunately, these amplifiers have a relatively small bandwidth, and cannot be used to amplify these short pulses.
As mentioned in Section 6.1, the time-of-flight distribution function has a width of typically 410 ps during the discharge. This width has two origins. First, the CFD is not perfect. Therefore, the time-of-flight measurement will still depend on the pulse amplitude. Second, density fluctuations will cause a spread in the flight time. Calculations show that a fluctuation level of about 4% in the local density could already explain the spread in the flight time, even with a perfectly working CFD. In general both effects will occur and the spread will come from a combination of these effects.

8 Proposal for a JET pulsed radar system

Any reflectometer system that is going to be implemented on the JET divertor has to match the already existing waveguide system. The in-machine components of the waveguide system have a square intersection with a size of 7 mm. This means that the lowest frequency that can be applied is 27 GHz. At this moment it is not yet clear what density can be reached in the divertor region. If we assume that a density of 5×10^{19} m^{-3} can be reached in front of the reflectometer antenna, then the maximum frequency needed to probe the plasma is about 60 GHz.
The waveguide system at JET has a round trip loss of ± 70 dB. For a resolution in the time of flight of ± 70 ps using pulses of about 1 ns, a SNR of 23 dB is needed (see Eq. (5.5)). The spectral noise power of a heterodyne system will be the same as for the RTP system, and is 2×10^{-20} W/Hz. Because the losses in the waveguide system will be higher for the transmission line to the JET divertor then for the transmission line used at RTP, the noise originating from the plasma can be neglected. Using (5.4), the signal power after the mixer is calculated to be 2.7×10^{-8} W. The mixer has a conversion loss of about 7 dB. Together with the loss in the waveguide (70 dB), the signal power that is coupled into the waveguide system must be 1.5 W. (This without taking pulse broadening into account.)
The pulse width to be used for a pulsed radar system at JET will be a trade-off between the achievable pulse power, the pulse length measured in real space, and the pulse broadening in

the divertor plasma. The maximum pulse length will be twice the distance between the antenna and the plasma. At this moment it is not clear how large this distance will be, but a maximum estimate will be in the order of 30 cm. This would mean a FWHM of 2 ns. The minimum pulse width is set by the pin switch, and is ± 700 ps. Using Eqs (5.4) and (5.5), the minimum pulse power needed to achieve a resolution of 70 ps can be calculated for the JET system. Using Eq. (2.8), the pulse broadening can be calculated for a parabolic density profile. In Fig. 8.1 the pulse broadening for reflection at 20% of the minor radius is shown.
The pulse amplitude diminishes because of the pulse broadening. This effect is taken into account in Fig. 8.1, and shows up as a non-linearity of the minimum needed pulse power as a function of the transmitted pulse width. From Fig. 8.1 it follows that a transmitted pulse with a pulse width of 0.9 ns and a amplitude of ± 1.6 W seems a reasonable trade-off between low distortion and minimum needed power.

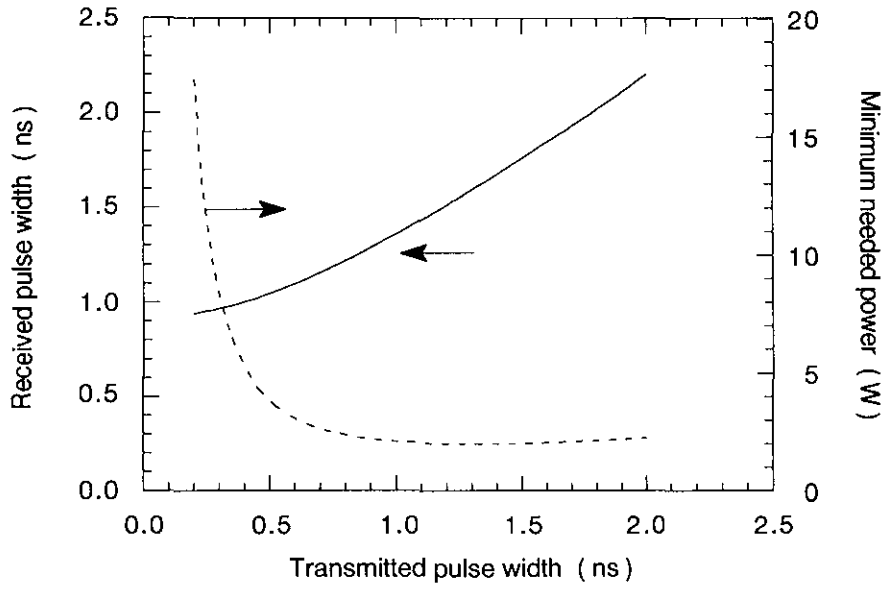

Fig. 8.1: Minimum needed pulse power as a function of the pulse width to get a resolution in the time of flight of 70 ps.

In principle there are two ways to generate pulses with these specifications. One way is to generate low-power pulses followed by a high-power Traveling Wave Tube Amplifier (TWTA). The other way is to use high-power modulated sources. Both methods have their drawbacks. The phase characteristic of a TWTA is nonlinear. This will lead to pulse deformations. At this moment it is not yet clear how severe this will be. Probably it will be possible to linearize the phase characteristic. If a TWTA can be used the output power can be amplified to about 100 W in the Ka-band. Directly modulated sources will have pulse widths in the order of a few nanoseconds. This means that a higher SNR is needed for the same resolution. Therefore, a higher output power is needed. Both methods will be discussed. In

Section 8.1 a general design of the pulsed radar system will be given. In Section 8.2 the system that makes use of a TWTA will be discussed in more detail. This system will be further referred to as the TWTA system. The second system, further referred to as the pulsed-sources system, will be discussed in Section 8.3. Prices of a system for JET are given in Section 8.4.

8.1 General design

The design of the JET pulsed radar system will be based on eight frequencies running from 27 to 60 GHz. So densities from 0.9×10^{19} to 4.5×10^{19} m^{-3} can be probed. The frequencies are chosen in such a way that they are equally distributed over two waveguide bands with designators: WG-22 (Ka-band), and WG-24 (U-band). The frequencies and the probing densities are presented in Table 8.1.1.

channel number	frequency ($\times10^9$ Hz)	critical density ($\times10^{19}$ m^{-3})
1	27.0	0.9
2	31.0	1.2
3	35.5	1.7
4	40.0	2.0
5	45.0	2.5
6	50.0	3.1
7	55.0	3.7
8	60.0	4.5

Table 8.1.1: Design frequencies and corresponding probing density and channel number as used in the text.

A block diagram of the complete pulsed radar system is shown in Fig. 8.1.1.

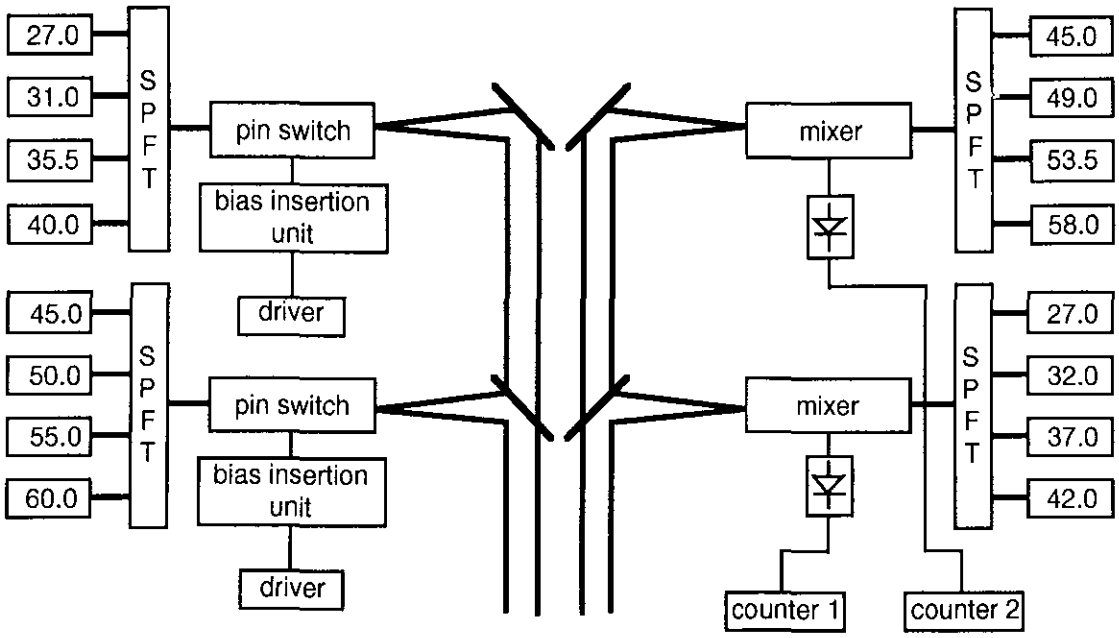

Fig. 8.1.1: Block diagram of the JET pulsed radar system.

The total system can again be separated into two major parts, namely the transmitter and the receiver. Both the transmitter and the receiver can be divided into two blocks of four channels. These blocks can be built in the same way as the RTP system. The two blocks are combined into one waveguide using oversized beam splitters. These have an insertion loss of -3 dB. As this loss also occurs in the receiver, a pulse power of 6.5 W is needed. If the oversized beam splitter is made frequency dependent, less loss is possible and the needed power is lowered. The power of 6.5 W, is the lower limit for reliable operations. Therefore, it is advisable to have some reserve and use pulses with a power of 60 W.

No matter whether the TWTA system or the pulsed-sources system will be built, the receiver for both systems remains the same. Heterodyne detection with an intermediate frequency (IF) of 18 GHz is used. Before detection the output signal of the mixer must be filtered and amplified. Using pulses with a power of 60 W, the gain of this amplifier must be 27 dB. After detection a video amplifier will be used. The detector will be operated in the squared law region between -40 and -10 dBm. The detector has a sensitivity of 1.4 V/mW, if it is loaded with a 1 MΩ impedance. The rise time of a detector is depending on both detector characteristics and load characteristics, and is given by:

$$t_{rise} = 2.2 \frac{R_V R_l}{R_V + R_l} (C_V + C_l), \tag{8.1}$$

with: R_V = video impedance, R_l = load impedance, C_V = detector bypass capacitor and C_l = load capacitor. The video impedance is typically 1 kΩ. Because of the long rise time, 700 ps for 1 ns pulses, and the low bypass capacitor, 0.5 pF, the video amplifier can have an

input impedance of 500 Ω. This will degrade the sensitivity to 470 mV/mW. Therefore, the output voltage is estimated to be between 50 μV and 50 mV. The CFD which is the input of the time-interval counter, needs a minimum signal of 30 mV and a maximum signal of 5 V. Hence, the video amplifier must have a gain of 100 times.
The counters are operated in the same way as described in Chapter 4, and need no further explanation.
By building the system in two bands, the Ka-band and the U-band, the total 8 point profile can be measured in 2 μs.

8.2 TWTA system

In this system normal Gunn oscillators are used to generate a CW signal. The pulse is than generated using pin diodes. Another possibility is to use so-called varactor modulators as designed by Dr Ermak from the Ukraine. From experience with the RTP system it became clear that each channel should have its own fast modulator with driver before the multi-throw switch. In this case the multi-throw switch can be replaced by a passive combiner network. The power needed for a system at JET is generated by a TWTA. This is a wide-band amplifier based on vacuum tube devices. These amplifiers have as a major limitation a nonlinear phase characteristic. This can lead to pulse shape deformations. At this moment it is not known how severe these deformations will be nor if it will be a problem for pulsed radar, but it is expected that a TWTA can be used. The output power of these amplifiers is in the order of 30 W at 60 GHz, and 100 W at 27 GHz, which would be sufficient for a JET-system. A schematic representation of the TWTA transmitter is shown in Fig. 8.2.1.

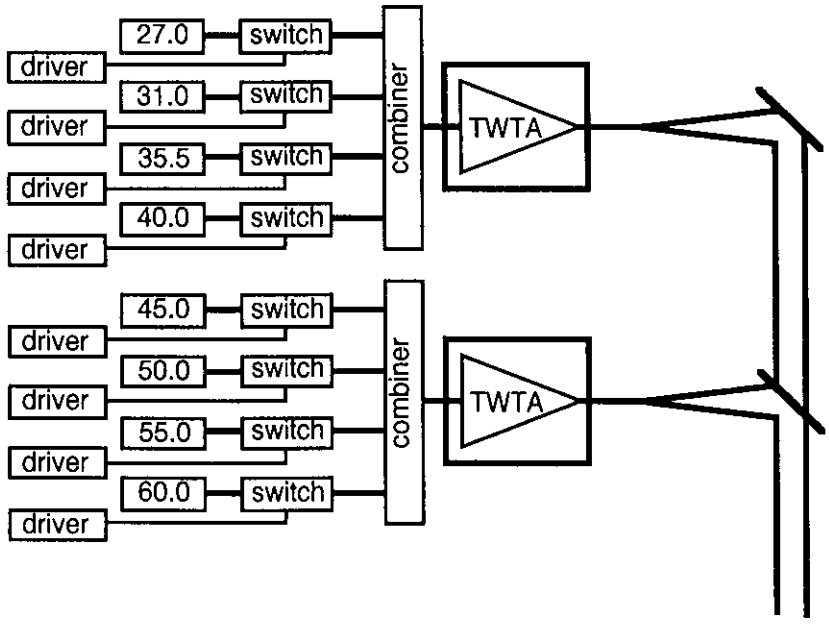

Fig. 8.2.1: The TWTA-transmitter.

8.3 Pulsed sources system

The pin switches used to modulate the CW signal cannot handle more than 1 W. If the signal has already been modulated, the maximum power on these switches can be increased to a few Watt. This is still not enough for JET. Therefore, if pulsed sources are used, these sources have to be directly modulated into pulses of 1 ns. The SPFT switch has to be replaced also. This can be done by a passive combiner circuit.
If pulses of a few ns can be accepted, it is possible to use pulsed Extended Interaction Oscillators (EIO). These are klystron-like oscillators capable of generating nanosecond pulses. The output power of these oscillators can be in the order of kilowatts up to frequencies of 220 GHz.

8.4 Costs

It is very difficult to give the exact price of a pulsed radar system at this moment. Therefore, the following quotations are only for the microwave parts and for the electronics to measure the flight time. Prices do not include data acquisition, software and infrastructure for operations at JET, and will be quoted in US$ because almost all offers have been given in that currency.
The receiver of the two proposed systems is the same and consists of eight oscillators with 17 dBm output power, two SPFT switches, two mixers, two IF preamplifiers with bandpass filters, two detectors and two video amplifiers. The prices of these components are listed in Table 8.4.1.

Oscillators (17 dBm+isolators)	40,000
SPFT Ka-band	10,000
SPFT U-band	12,000
2 mixers	10,000
2 IF pre ampl.	12,000
2 detectors	4,000
2 video ampl.	2,500
waveguide components	20,000
2 counters	50,000
Total	160,500

Table 8.4.1: Costs of the receiver in US$.

In the same way the price of the two transmitter systems can be estimated. The TWTA system uses eight oscillators, eight fast modulators, two combiner networks, eight drivers, a TWTA in

Ka-band and a TWTA in U-band. The prices of the different components in the transmitter of the TWTA system are listed in Table 8.4.2.

8 oscillators (17 dBm+isolators)	40,000
8 fast pin switches	32,000
combiner in Ka-band	**8,000***
combiner in U-band	**10,000***
8 drivers	30,000
TWTA in Ka-band (100 W)	100,000
TWTA in U-band (30 W)	**150,000***
waveguide components	20,000
Total	390,000

Table 8.4.2: Costs of the transmitter for the TWTA system in US$.
** indicates estimated costs without firm offer.*

The pulsed-sources system uses eight pulsed high-power oscillators, and two combiners. The prices of the transmitter of the pulsed-sources system are listed in Table 8.4.3.

8× high-power sources incl drivers	**800,000***
2× combiners	**20,000***
waveguide components	20,000
Total	840,000

Table 8.4.3: Costs of the transmitter for the pulsed-sources system in US$.
** indicates estimated costs without firm offer.*

The total cost for a pulsed radar system at the JET divertor is therefore estimated to be US$ 550,500 if the TWTA system will be built, and US$ 1,000,500 if the pulsed-sources system will be built.

9 Conclusions

In this report the layout of a pulsed radar system as developed for use at the RTP tokamak has been described and some experimental results have been discussed. Also, a very fast high resolution counter system has been designed. It is shown that the resolution of the counter is improved by employing several counters parallel. The complete counter system is expected to become operational in March 1994.

On base of the experience gained with the RTP system, a design of a pulsed radar system for the JET new phase divertor is given. Although there are many ways of designing such a system, only two designs are suggested here. They are based on the assumption that an eight points density profile must be measured in 2 μs. The cost of components for the cheapest option of the two would be about 0.5 MECU. If specifications will change at the time of final design, it could be possible to choose a completely different approach e.g. by using BWOs.

Acknowledgements

The authors wish to thank the RTP team and especially the Interferometer group and the Thomson-scattering group for making available their results.
This work was performed under article 14 contract no. JE2/9001 and as part of the research programme of the association agreement of Euratom and the "Stichting voor Fundamenteel Onderzoek der Materie" (FOM) with financial support from the "Nederlandse Organisatie voor Wetenschappelijk Onderzoek" (NWO) and Euratom.

References

Binds-93 H. Bindslev, "On the theory of Thomson scattering and reflectometry in a relativistic magnetized plasma", Thesis Department of Engineering Science, Oxford (1992)

Budd-61 K.G. Budden, "Radio waves in the ionosphere", University Press, Cambridge (1961)

EG&G-82 EG&G Ortec;
AN-42: "Principles and Applications of Timing Spectroscopy", (1982).

Ginz-60 V.L. Ginzberg, "The propagation of electromagnetic waves in plasma", Pergamont Press, Oxford (1970)

Okre-68 E.C. Okress, "Microwave power engineering", Academic Press, New York (1968)

Some additional remarks

In chapter 8.3, a pulsed radar system is described, based on using directly pulsed high-power oscillators. These high-power oscillators are vacuum tube devices and can only generate pulses with a FWHM of several nanoseconds. Besides this, these oscillators are also very expensive, about $100,000 each. In the mean time it is shown that solid state oscillators can generate pulsed powers of 100 W in Ka-band with a pulse rise time less than 300 ps.*) A system based on these oscillators can be a good alternative to the TWTA system., especially because in this case no vacuum tube devices are used, and only low voltage power supplies are needed, making the system more reliable. The exact prices of the solid state oscillators are not yet known. A 30 W oscillator in Ka-band without power supply is quoted to cost $6,000. Therefore, it is expected that a 60 W oscillator including power supply will cost about $20,000. So, the cost of an eight-channel pulsed-sources system will be $200,000 for the transmitter and $160,500 for the receiver, making a total cost of $360.500. This is about the same price as that of a TWTA system.

*) Dr. G. Ermak, Institute of Radiophysics and Electronics of the Ukraine, Ak. Proskura st. 12, Kharkov 310085, Ukraine.